ADVANCED ENGINEERING MATERIALS

DOI: 10.1002/adem.201600058

Texture Development in Cold Deformed and Recrystallized Ti–30Nb–4Sn Alloy and Its Effects on Hardness and Young's Modulus**

By *Leonardo Fanton, Nelson Batista de Lima, Alexandra de Oliveira França Hayama, Rubens Caram* and *João Batista Fogagnolo**

This study analyzes the effects of cold deformation and recrystallization on the microstructure, texture evolution, and mechanical properties of Ti–30Nb–4Sn alloy. The samples are cold rolled to reduce their thickness by up to 85%. The most deformed sample is subjected to recrystallization treatment. The crystallographic texture is determined by X-ray pole figures. The 51% deformed sample shows a {203}<010> texture. The 85% deformed sample shows two texture components: {203}<010> and {130}<-310>, while the recrystallized sample shows a fiber texture with the {130} plane parallel to the sample surface. Hardness increases and Young's modulus tends to decrease in response to increasing deformation. The recrystallized sample shows low hardness and Young's modulus.

1. Introduction

Titanium alloys offer high specific strength and excellent corrosion resistance. These characteristics make titanium alloys an excellent choice for the aerospace sector and medical engineering.[1] One of the main problems with using metallic implants for bone replacement is their relatively high Young's modulus. The higher stiffness of a prosthesis reduces the stress applied on the bone. According to Wolff's law, the bone remodels itself in response to the load exerted on it and its density may be reduced (osteopenia) if not properly stimulated.[2] This phenomenon, called the "stress shielding" effect, could be reduced if the prosthesis was made of alloys with Young's modulus closer to that of bone (10–40 GPa).[3]

Beta (β) titanium alloys exhibit lower stiffness than other orthopedic alloys commonly used, such as stainless steel (200 GPa), Co–Cr–Mo alloys (200–230 GPa), and Ti–6Al–4V (110 GPa).[3,4] While pure titanium has a modulus of about 110 GPa,[5] some Ti–Nb, Ti–Mo, and other β alloys can reach values as low as 50 GPa.[6–14] The Young's modulus of titanium alloys strongly depends on their phases. Lee et al.[15] studied Ti–Nb alloys with several different Nb contents. Considering the dominant phase obtained for each composition, they proposed the following sequence for the elastic modulus of titanium phases: $\omega > \alpha > \alpha' > \alpha'' > \beta$. In another study on Ti–Mo alloys, Ho et al.[8] suggested that the Young's modulus of α″ phase is lower than that of β phase.

As α″ and β have the lowest values of Young's modulus, titanium alloys based on these phases are a good choice when low stiffness is required. In many applications, the stress applied on a part is concentrated in a given direction. Since these phases have a crystallographic anisotropy of elastic properties, the Young's modulus of a polycrystalline alloy could be controlled in a specific direction by controlling the texture (preferred orientation). Deformation and recrystallization are two common ways to create texture on metal alloys. Several studies have focused on the texture of β[16–28] and α″ phases[17,18,20,27–29] in titanium alloys. Nevertheless, α″ phase appears to have received less attention, particularly in terms of recrystallization texture. This study analyzes the development of texture in cold rolled and recrystallized Ti–30Nb–4Sn

[*] *Dr. J. B. Fogagnolo, Dr. L. Fanton, Dr. R. Caram*
State University of Campinas, Rua Mendeleyev, 200, Campinas 13083-860, Sao Paulo, Brazil
E-mail: fogagnolo@fem.unicamp.br
Dr. N. B. de Lima
Instituto de Pesquisas Energéticas e Nucleares, Avenida Lineu Prestes, 2242, São Paulo-SP 05508-000, Brazil
Dr. A. d. O. F. Hayama
Universidade Federal do Mato Grosso, Avenida Fernando Corrêa da Costa, 2367, Cuiabá-MT 78060-900, Brazil

[**] *This work was supported by the Brazilian funding agencies CAPES (Federal Agency for the Support and Improvement of Higher Education), CNPq (National Council for Scientific and Technological Development), and FAPESP (São Paulo State Research Foundation – Grant 2011/19982-2) for financial support.*

Table 1. Composition of the alloy determined by XRF.

Element	Nb	Sn	O_2	N_2	Ti
Content [mass%]	29.2	3.9	0.13	0.0045	Balance
Std dev	0.2	0.1	0.004	0.00035	

alloy, as well as its effects on the material's hardness and modulus of elasticity.

2. Experimental Secttion

The Ti–30Nb–4Sn alloy sample was sealed in quartz glass and processed by electric arc melting in an argon atmosphere, followed by homogenization at 1 000 °C for 8 h and water quenching at room temperature. The homogenized ingot was chemically analyzed in three different regions. The composition of the alloy was examined by X-ray fluorescence spectroscopy (XRF) (Rigaku RIX3100), while nitrogen and oxygen levels were evaluated using a gas analyzer (LECO-TC400).

The ingot was deformed by cold rolling in multiple passes to prevent adiabatic heating. Samples with different degrees of deformation were obtained: 24, 36, 51, 68, 79, and 85% thickness. The deformation of the homogenized sample was considered to be 0%. To investigate the effect of recrystallization on the texture, an 85% deformed sample was heat treated at 800 °C for 30 min in argon atmosphere and then water quenched at room temperature; this sample is hereinafter referred to as 85% HT.

Metallographic specimens were prepared using diamond paste followed by colloidal silica suspension and etching with Kroll reagent. The grain size of the recrystallized sample (85 HT)

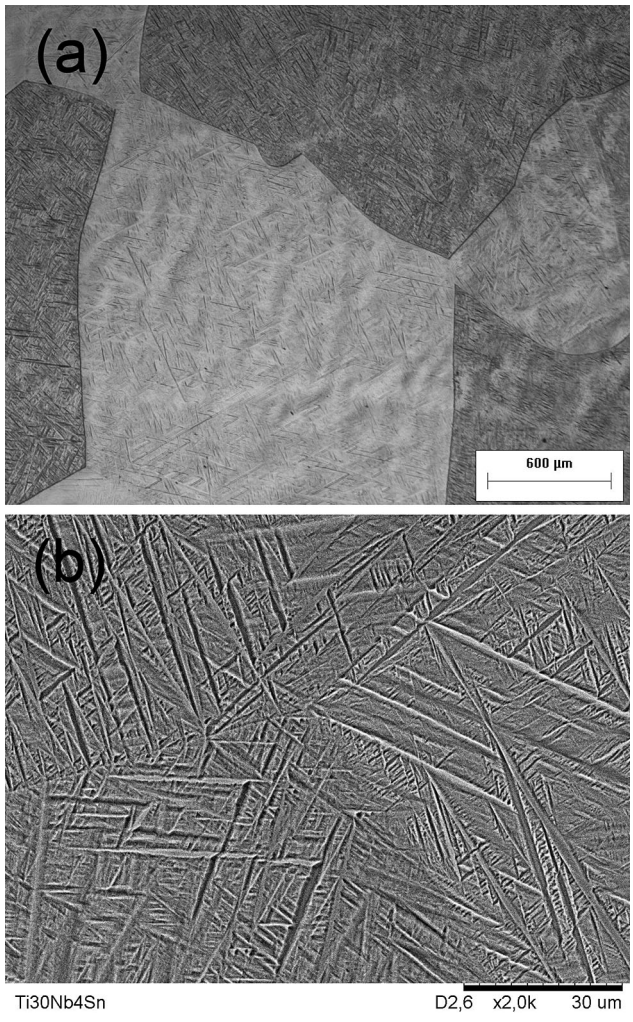

Fig. 1. Light microscopy images of a homogenized sample.

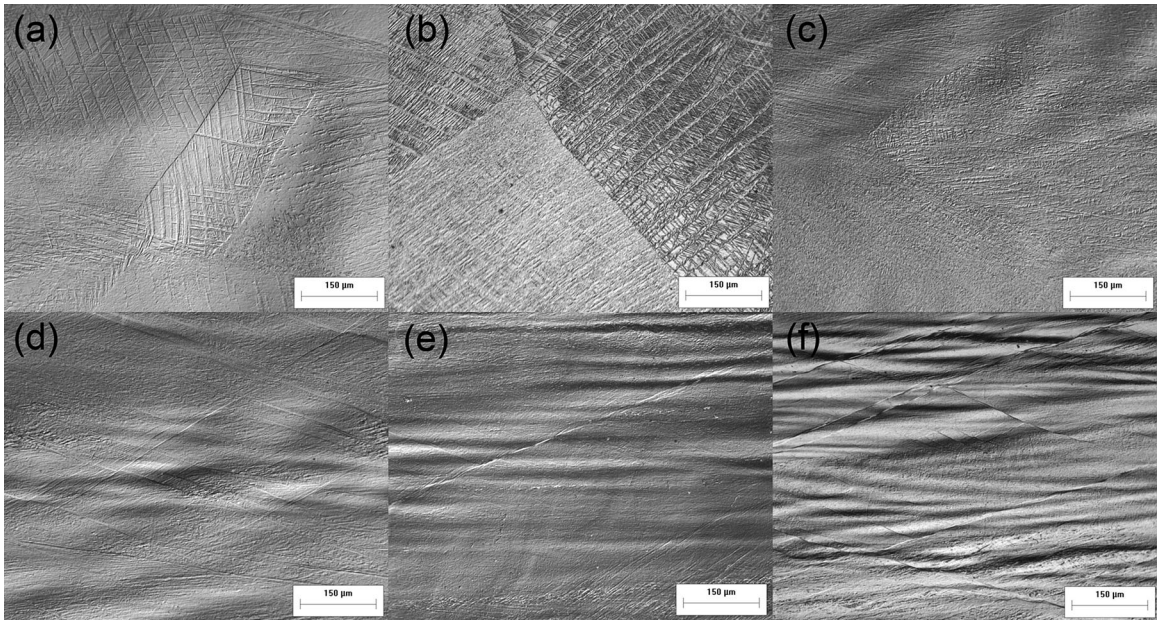

Fig. 2. Light microscopy images of cold-rolled samples with deformations of: (a) 24, (b) 36, (c) 51, (d) 68, (d) 79, and (e) 85%.

ADVANCED ENGINEERING MATERIALS

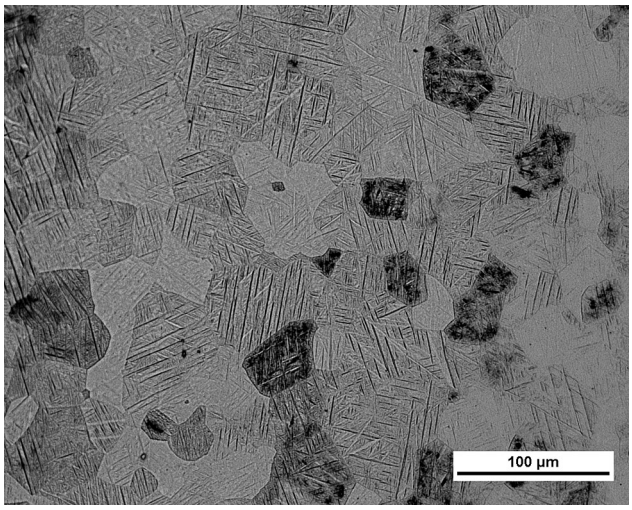

Fig. 3. Light microscopy image of the 85% HT sample.

was measured in accordance with ASTM E112 standard. Vickers microhardness (HV) was measured with a Buehler Micromet 2100 hardness tester, applying a load of 1 N for 30 s. At least 10 measurements were taken of each sample. The X-ray diffraction (XRD) analysis was performed in a PANalytical X'Pert PRO diffractometer equipped with a Cu-Kα radiation source. The pole figures for texture analysis were obtained with a Rigaku X-ray diffractometer equipped with a texture goniometer. The Young's modulus was determined by the ultrasonic method, using a Panametrics-NDT 5072PR pulser-receiver with 5 MHz transducers, as specified by the ASTM E494-10 standard. The sound waves were emitted in the normal direction of the sample.

3. Results and Discussion

The composition of the alloy determined by X-ray fluorescence spectroscopy (XRF) is described in Table 1. As can be seen, the Nb and Sn contents are very close to the nominal composition. Although there is no standard for maximum allowable oxygen and nitrogen levels for this class of alloy, the values obtained here can be considered low. The ASTM F67-06 standard for titanium grade 2 specifies a maximum of 0.25 and 0.03% for oxygen and nitrogen, respectively.

Figure 1 depicts the microstructure of the homogenized Ti–30Nb–4Sn alloy after quenching. The low-magnification image (Figure 1a) shows a microstructure composed of coarse grains of about 3 mm, while the high-magnification image (Figure 1b) reveals the martensitic microstructure. Moraes et al.[30] reported the presence of α″ orthorhombic martensitic phase in the same alloy. This phase is usually formed in the presence of a large amount of β stabilizer elements, but not sufficient to fully stabilize the β phase. For Ti–Nb alloys, this is the equivalent to approximately 13–36 wt% of niobium.[31]

Figure 2 illustrates the microstructural evolution after cold rolling. Samples with 24–51% of deformation show clearly visible grain boundaries. However, from 68 to 85% of deformation, the grains become very elongated and aligned in the rolling direction. Deformation heterogeneities such as shear bands are also visible on the three most deformed samples (thickness reduction of 68, 79, and 85%). Hayama et al.[20] reported similar results for Ti–35Nb alloy in the undeformed state after different degrees of cold deformation. The microstructure of the 85% HT sample (Figure 3) reveals a significant reduction in grain size to about 37 μm (ASTM grain size number 6.6).

Figure 4 shows the XRD patterns of Ti–30Nb–4Sn alloy with different degrees of deformation. Some of the standard peaks of α″ [JCPDS X-ray Powder Diffraction File No. 17–102] and β [JCPDS X-ray Powder Diffraction File No. 89–3726] are plotted for comparison, since previous works[30,32] show that

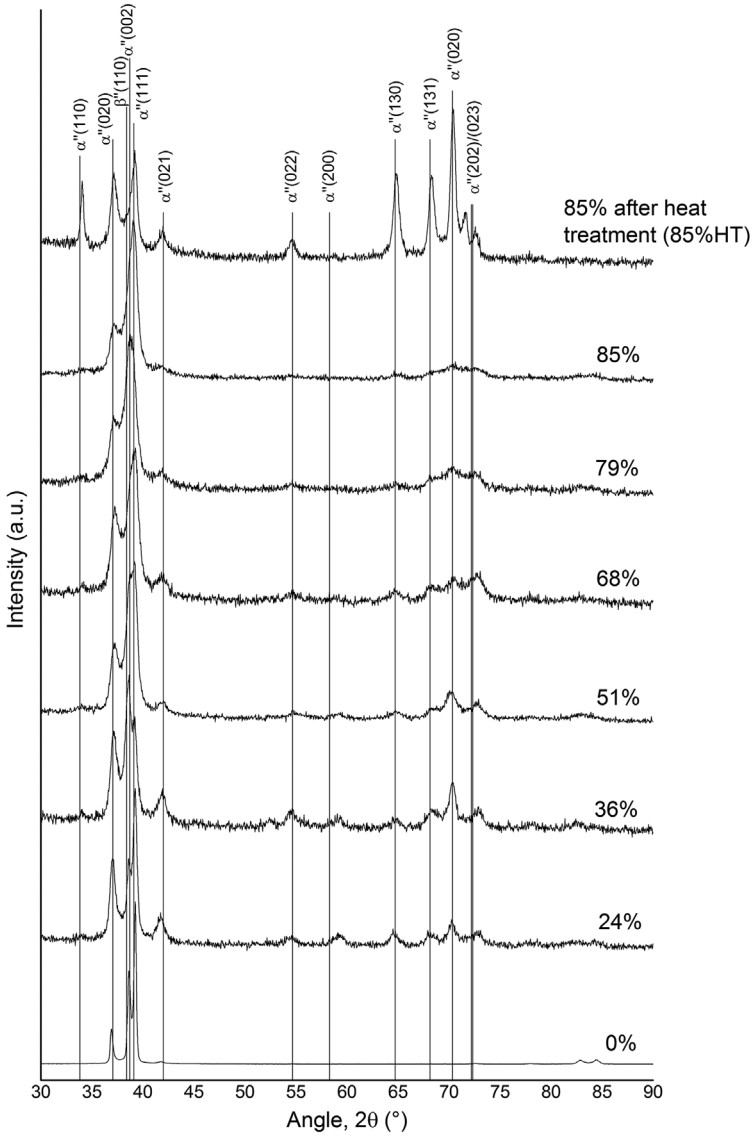

Fig. 4. XRD patterns of samples in different conditions.

these phases are expected in Ti–30Nb–4Sn alloy. Note that most of the peaks fit the α″ pattern quite well. However, β peaks are not clearly distinguishable, i.e., some of them appear to be absent while others are very close to other α″ peaks. Therefore, only α″ peaks will be used for texture analysis. The XRD analysis did not reveal ω phase. Moreover, it has been reported that ω phase precipitation is prevented by adding Sn to Ti–Nb alloys.[30] With increasing deformation, the XRD peaks became broader due to subgrain refinement and residual lattice distortion. The XRD pattern of the 85% HT sample revealed a change in the relative intensity of some α″ peaks, indicating a change in the texture in response to recrystallization.

Figure 5–7 show the pole figures obtained for the 51, 85, and 85% heat-treated samples, respectively. The 51% deformed sample showed a {203}<010> texture. The pole figures of the 85% deformed sample indicate that the {203}<010> texture was still present, and another texture component was also identified near {130}<-310>. After heat treatment, the 85% deformed sample showed a fiber-like texture with the {130} plane almost parallel to the surface of the sample. This fiber-like texture showed variations in intensity, the highest one appearing at {130}<-310>. Note that the textures were measured on the sample surface. Considering the deformation heterogeneities between the surface and inner parts after cold rolling, some variations in texture should be expected. It is important to mention that these textures have not been reported in any previous work.

The alignment of direction <010> along the rolling direction has already been observed for the α″ phase.[17,18,29] Matsumoto et al.[17,18] found {200}<010> and {220}<001> textures of α″ for Ti–Nb–Sn alloys. In a more recent work, Hayama et al.[20] reported {1-21}<-214> and {1-42}<213> textures for a Ti–35Nb alloy. One hypothesis for this difference is the presence of a different volume fraction of β phase before cold deformation. The latter authors reported textures in which the undeformed alloy presented a greater volume fraction of β phase, and the α″ phase was induced by deformation during cold rolling. In the case of the results of the present study, the XRD pattern of the undeformed sample indicates a preponderance of α″ phase induced by quenching.

Figure 8 illustrates the hardness and Young's modulus as a function of the degree of deformation. The hardness and Young's modulus of the 85% HT sample are also plotted. The undeformed material presented a hardness of 190 HV, which can be considered low compared to that of other α″-based alloys such as Ti–7.5Mo (263 HV)[8] and Ti–22.5Nb (300 HV).[15] When deformed, the material initially undergoes

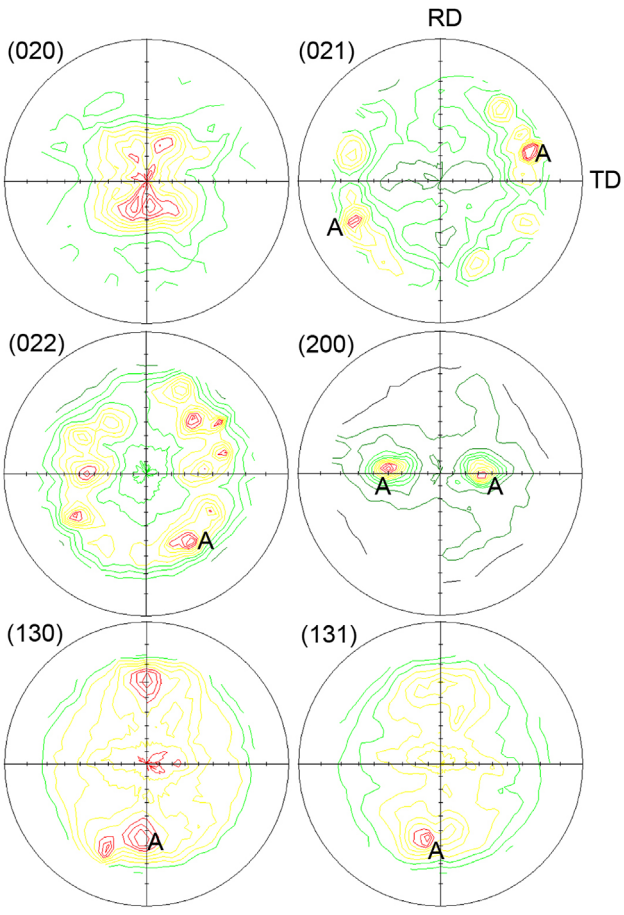

Fig. 5. Pole figures of the 51% deformed sample.

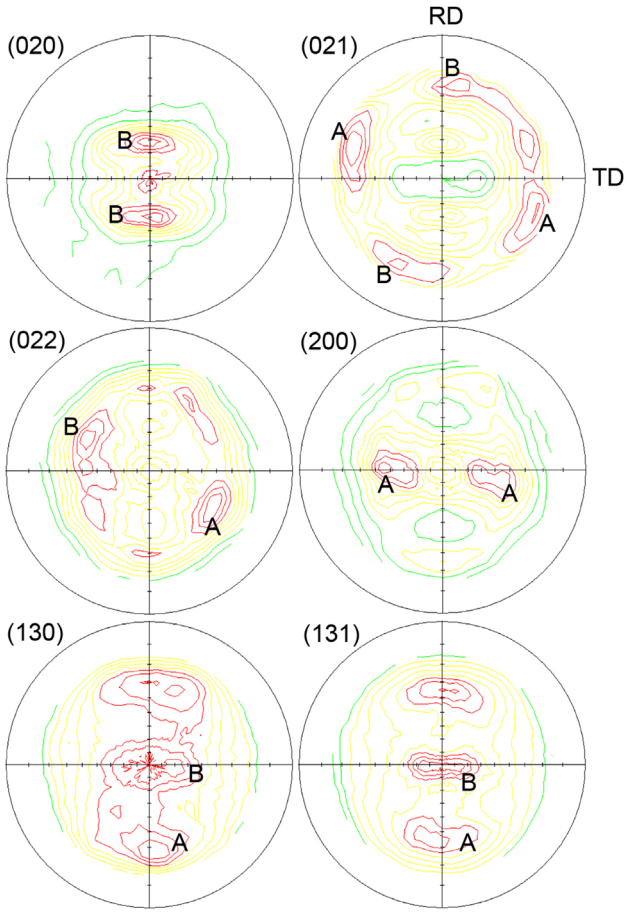

Fig. 6. Pole figures of the 85% deformed sample.

ADVANCED ENGINEERING MATERIALS

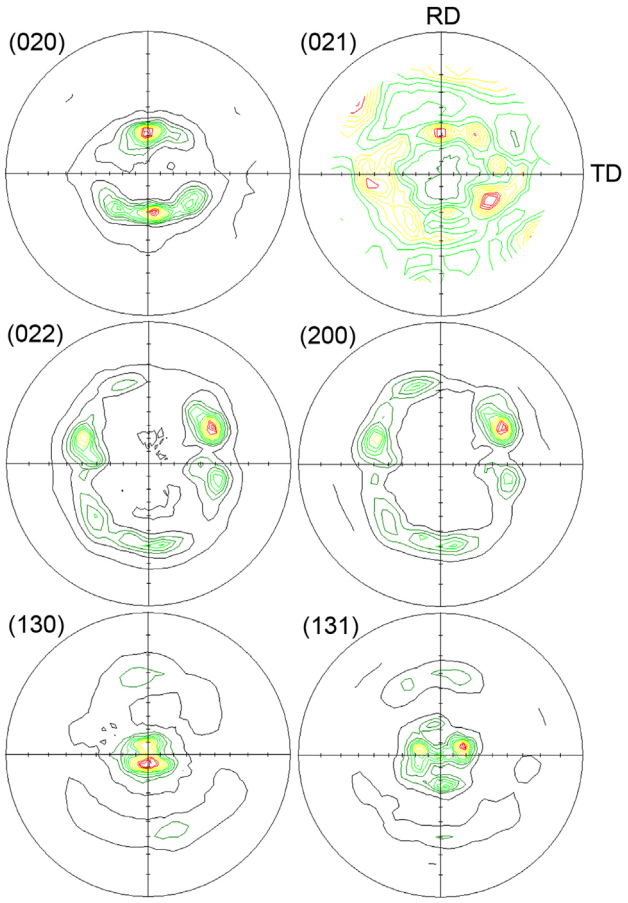

Fig. 7. Pole figures of the 85% heat-treated sample (85% HT).

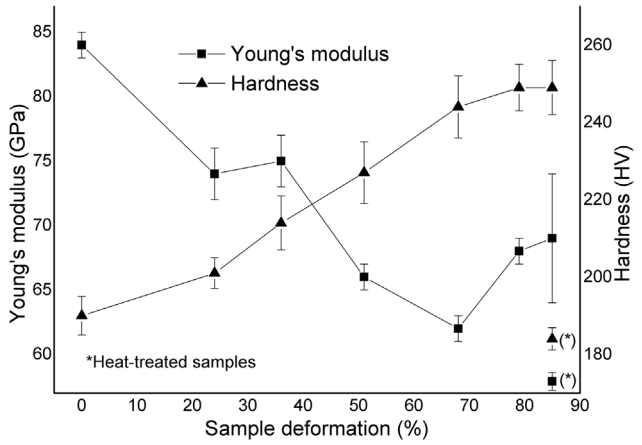

Fig. 8. Hardness and Young's modulus as a function of the sample's condition.

a rapid increase in hardness, reaching 244 HV in the 68% deformed material. This increase in hardness can be attributed to subgrain refinement, enhanced lattice distortion, and dislocation density.[33] The first two factors are confirmed by the XRD patterns, as stated earlier. After 68% of deformation, the hardness level appears to stabilize owing to work hardening, reaching 249 HV at 85% deformation. The hardness of the samples in the as-quenched and recrystallized states are similar, despite the smaller grain size of the recrystallized sample. The hardness levels found in this work are relatively similar to those of a previous study on Ti–35Nb alloy.[20]

The Young's modulus decreased in the samples deformed up to 24–51%, showing values of approximately 84–74 GPa. This tendency to decrease continued up a deformation of 68%, when the stiffness of the material was reduced to 62 GPa. In the last two degrees of deformation, the values increased again, reaching 69 GPa in the sample deformed up to 85%. The heat-treated samples presented decreasing hardness and Young's modulus, with values of 184 HV and 58 GPa, respectively.

Dai et al.[33] reported that the Young's modulus of Ti–35Nb–9Zr–6Mo–4Sn alloy (single β without α″ strain-induced transformation) decreased with increasing cold deformation. The authors attributed this decrease in Young's modulus to three factors: i) increase in grain boundaries due to grain refinement, ii) increase in dislocation density, and iii) texture. The first two factors can be explained by the fact that the growth of crystalline defects such as vacancies and dislocations may reduce the strength of atomic bonds, which in turn implies a reduced Young's modulus. The low Young's modulus of the recrystallized sample (low dislocation density), which is as low as that of the 68% deformed sample (high dislocation density), indicates that the entire texture factor is significant. Moreover, Kim and Bush[34] demonstrated that a considerable reduction in Young's modulus with grain refinement occurs only at grain sizes smaller than 10 nm. Considering that b is the largest lattice constant in the α″ orthorhombic structure, Young's modulus in the [010] direction should be smaller than in the [100] and [001] directions.[18] Sun et al.'s[35] theoretical calculations of the α″ elastic constants of Ti–25at%Nb alloy suggest that the differences in the elastic constants along these directions are negligible and that more significant variations should be expected in intermediary directions such as <111>. The use of different techniques to measure the texture and the Young's modulus, such as electron backscatter diffraction (EBSD) and nanoindentation, respectively, should be useful to corroborate the results of this work and to shed more light on the relationship between texture and Young's modulus in the Ti–30Nb–4Sn alloy.

4. Conclusions

The XRD patterns and light microscopy images indicated that the Ti–30Nb–4Sn alloy has high contents of α″ orthorhombic martensitic phase. The XRD pole figures of sample surfaces revealed a {203}<010> texture for the 51% deformed sample, {203}<010> and {130}<-310> for the 85% deformed sample, and a fiber texture for the 85% HT sample with the {130} plane parallel to the sample surface. These results allow for a better understanding of how the textures in this alloy can evolve through cold rolling and recrystallization. This study also demonstrates that work hardening occurs when thickness is reduced by about 68% and that the lowest Young's modulus can also be obtained with similar deformations. The recrystallization heat-treatment applied

here considerably reduced the stiffness of the alloy. Although the recent literature reports that the decrease in Young's modulus during deformation can be attributed to an increase in α″ crystalline defects and/or changes in texture, a better understanding of Young's modulus and the anisotropy of α″ in Ti alloys is still needed.

Article first published online: May 04, 2016
Manuscript Revised: March 31, 2016
Manuscript Received: January 30, 2016

[1] C. Leyens, M. Peters, *Titanium and Titanium Alloys*, Wiley-VCH Verlag GmbH & Co. KGaA, Weinheim, FRG **2003**.
[2] Y. Oshida, *Bioscience and Bioengineering of Titanium Materials*, Elsevier, Massachusetts, USA **2013**.
[3] B. Soumya, R. Nag, S. Nag, R. Banerjee, in *ASM Handbook*, ASM International, Ohio, USA **2012**, 6.
[4] G. Lutjering, J. C. Willians, *Titanium (Engineering Materials and Processes)*, Springer, New York **2007**.
[5] X. Liu, P. K. Chu, C. Ding, *Mater. Sci. Eng. R Rep*. **2004**, *47*, 49.
[6] F. F. Cardoso, P. L. Ferrandini, E. S. N. Lopes, A. Cremasco, R. Caram, *J. Mech. Behav. Biomed. Mater.* **2014**, *32*, 31.
[7] A. Almeida, D. Gupta, C. Loable, R. Vilar, *Mater. Sci. Eng. C* **2012**, *32*, 1190.
[8] W. F. Ho, C .P. Ju, J. H. Chern Lin, *Biomaterials* **1999**, *20*, 2115.
[9] V. Brailovski, S. Prokoshkin, M. Gauthier, K. Inaekyan, S. Dubinskiy, M. Petrzhik, M. Filonov, *Mater. Sci. Eng. C* **2011**, *31*, 643.
[10] Y. L. Zhou, M. Niinomi, T. Akahori, *Mater. Sci. Eng. A* **2004**, *371*, 283.
[11] N. Sakaguchi, M. Niinomi, T. Akahori, J. Takeda, H. Toda, *Mater. Sci. Eng. C* **2005**, *25*, 370.
[12] M. Popa, J. M. C. Moreno, C. Vasilescu, S. I. Drob, E. I. Neacsu, A. Coer, J. Hmeljak, G. Zerjav, I. Milošev, *Metall. Mater. Trans. A* **2014**, *45*, 3130.
[13] D. R. N. Correa, P. A. B. Kuroda, C. R. Grandini, *Adv. Mater. Res*. **2014**, *922*, 75.
[14] D. Kent, G. Wang, M. Dargusch, *J. Mech. Behav. Biomed. Mater.* **2013**, *28*, 15.
[15] C. M. Lee, C. P. Ju, J. H. C. Lin, J. H. C. Lin, *J. Oral Rehabil*. **2002**, *29*, 314.
[16] T. Inamura, H. Hosoda, K. Wakashima, S. Miyazaki, *Mater. Trans*. **2005**, *46*, 1597.
[17] H. Matsumoto, S. Watanabe, S. Hanada, *Mater. Trans*. **2005**, *46*, 1070.
[18] H. Matsumoto, S. Watanabe, S. Hanada, *J. Alloys Compd*. **2007**, *439*, 146.
[19] M. Abdel-Hady, in *Recent Developments in the Study of Recrystallization*, InTech, Croatia **2013**, 20.
[20] A. O. F. Hayama, J. F. S. C. Lopes, M. J. G. da Silva, H. F. G. Abreu, R. Caram, *Mater. Des*. **2014**, *60*, 653.
[21] A. K. Singh, R. A. Schwarzer, *Trans. Indian Inst. Met*. **2008**, *61*, 371.
[22] Y. Chen, J. Li, B. Tang, H. Kou, X. Xue, Y. Cui, *J. Alloys Compd*. **2015**, *618*, 146.
[23] B. Sander, D. Raabe, *Mater. Sci. Eng. A* **2008**, *479*, 236.
[24] T. A. Sokolova, L. I. Anisimova, B. K. Sokolov, *Textures Microstruct*. **1999**, *32*, 101.
[25] Y. Yang, P. Castany, M. Cornen, I. Thibon, F. Prima, T. Gloriant, *J. Alloys Compd*. **2014**, *591*, 85.
[26] W. Cui, A. Guo, L. Zhou, C. Liu, *Sci. China Technol. Sci*. **2010**, *53*, 1513.
[27] S. Hanada, N. Masahashi, T. K. Jung, M. Miyake, Y. S. Sato, H. Kokawa, *J. Mech. Behav. Biomed. Mater*. **2014**, *32*, 310.
[28] S. Hanada, N. Masahashi, T. K. Jung, N. Yamada, G. Yamako, E. Itoi, *J. Mech. Behav. Biomed. Mater.* **2014**, *30*, 140.
[29] S. Hanada, N. Masahashi, T. K. Jung, *Mater. Sci. Eng. A* **2013**, *588*, 403.
[30] P. E. L. Moraes, R. J. Contieri, E. S. N. Lopes, A. Robin, R. Caram, *Mater. Charact*. **2014**, *96*, 273.
[31] A. Cremasco, Deformação Plástica a Frio, Transformações de Fases E Propriedades Mecânicas de Ligas Ti-Nb-Sn Para Uso Biomédico Deformação Plástica a Frio, Transformação de Fases E Propriedades Mecânicas de Ligas Ti-Nb-Sn Para Uso Biomédico, University of Campinas, Campinas-SP, Brazil **2012**.
[32] T. Ozaki, H. Matsumoto, S. Watanabe, S. Hanada, *Mater. Trans*. **2004**, *45*, 2776.
[33] S. Dai, Y. Wang, F. Chen, X. Yu, Y. Zhang, *Mater. Sci. Eng. A* **2013**, *575*, 35.
[34] H. S. Kim, M. B. Bush, *Nanostructured Mater.* **1999**, *11*, 361.
[35] J. Sun, Q. Yao, H. Xing, W. Y. Guo, *J. Phys. Condens. Matter* **2007**, *19*, 486215.

